Applied Physics Letters ARTICLE pubs.aip.org/aip/apl

Long-range superconducting proximity effect in $YBa_2Cu_3O_7/La_{0.7}Ca_{0.3}MnO_3$ weak-link arrays

Cite as: Appl. Phys. Lett. **124**, 222603 (2024); doi: 10.1063/5.0189305
Submitted: 22 December 2023 · Accepted: 21 May 2024 ·
Published Online: 30 May 2024 · Corrected: 6 June 2024

D. Sanchez-Manzano,[1,a] S. Mesoraca,[2] S. Rodriguez-Corvillo,[1] A. Lagarrigue,[2] F. Gallego,[1] F. A. Cuellar,[1] A. Sander,[2] A. Rivera-Calzada,[1] S. Valencia,[3] J. E. Villegas,[2] C. Leon,[1] and J. Santamaria[1]

AFFILIATIONS

[1]GFMC, Departamento de Física de Materiales, Facultad de Ciencias Físicas, UCM, Plaza Ciencias, 1, 28040 Madrid, Spain
[2]Laboratoire Albert Fert, CNRS, Thales, Université Paris-Saclay, 91767 Palaiseau, France
[3]Helmholtz-Zentrum Berlin für Materialien und Energie, Albert-Einstein-Str. 15, 12489 Berlin, Germany

[a]Author to whom correspondence should be addressed: davidsan@ucm.es

ABSTRACT

The interplay between ferromagnetism and superconductivity has attracted substantial interest due to its potential for exotic quantum phenomena and advanced electronic devices. Although ferromagnetism and superconductivity are antagonistic phenomena, ferromagnets (F) can host spin-triplet superconductivity induced via proximity with superconductors (S). To date, most of the experimental effort has been focused on single S/F/S junctions. Here, we have found the fingerprints of long-range superconducting proximity effect in micrometric weak-link arrays, formed by embedding $YBa_2Cu_3O_7$ superconducting islands in a half-metallic ferromagnet $La_{0.7}Ca_{0.3}MnO_3$ film. These arrays show magnetoresistance oscillations that appear at temperatures below the critical temperature of $YBa_2Cu_3O_7$ for currents below a threshold, indicating their superconducting origin. This realization paves the way for device architectures displaying macroscopic quantum interference effects, which are of interest for field sensing applications, among others.

The possible coexistence of ferromagnetism (FM) and superconductivity (SC) has attracted interest for many years.[1] Singlet superconductivity (SC) and ferromagnetism (FM) are antagonistic phenomena because the exchange field of an F tends to spin-polarize Cooper pairs' electrons with opposite spins. The recent discovery of superconductivity in a P-doped $EuFe_2As_2$ compound[2] with extremely weak exchange interaction between electrons and localized moments is a rare case of coexistence of ferromagnetism and singlet superconductivity. Another possibility for F/S coexistence is spin-triplet superconductivity. Here, equal-spin Cooper pairs can survive over long distances in ferromagnets. Triplet pairing is also very rare as an intrinsic phenomenon, and has only been observed in uranium compounds.[3–6] However, it has been theoretically and experimentally demonstrated that triplet correlations can emerge at the interface between a ferromagnet (F) and a superconductor (S) resulting from the presence of inhomogeneous magnetization,[7–9] non-collinear magnetizations in ferromagnetic multilayers,[10,11] and spin-dependent scattering or momentum-dependent exchange fields due to the spin–orbit interaction.[12–14] In experiments with both conventional low-temperature superconductors and high-temperature superconductors, supercurrents have been observed across S–F–S junctions in which F thickness is in the tens of nanometer range,[15–20] significantly exceeding the expectations for the singlet S–F proximity effect, thereby supporting the triplet scenario. Additionally, lateral (planar) devices based on half-metallic ferromagnets (like CrO_2 and $La_{0.7}Sr_{0.3}MnO_3$) have exhibited supercurrents decaying over even longer distances, up to micrometers, which strongly indicates proximity-induced triplet superconductivity.[21–25] All those realizations have paved the way to the so-called superconducting spintronics. This research field, at the intersection of superconductivity and ferromagnetism, has garnered significant attention due to its potential for quantum computing[26] and sensing,[17] and for the exploration of exotic quantum phenomena.[27]

Most of the studies on S/F proximity effects have focused on individual S/F/S junctions and multilayers. Yet, for nonmagnetic systems, a different type of 2-dimensional (2D) proximity structures has been explored which consists of superconducting islands embedded, e.g., on metallic,[28] semiconducting[29,30] or insulating films.[31] In these structures, superconductivity is induced around the superconducting

islands by proximity effect, which allows the global propagation of superconducting correlations across all the embedding material, the space between the S islands behaving as weak links. Such 2D weak-link arrays constitute an interesting platform for studying a variety of physics problems that span from Berezinskii–Kosterlitz–Thouless (BKT) transitions to dimensional or geometric frustration effects.[32,33] In this paper, we explore the long-range superconducting proximity effect in 2D weak-link in which the proximitized materials is a ferromagnet. In particular, we investigate arrays based on the high-temperature superconductor $YBa_2Cu_3O_7$ (YBCO) and the half-metallic ferromagnetic $La_{0.7}Ca_{0.3}MnO_3$ (LCMO). We find macroscopic superconducting quantum interference effects that dominate magnetotransport despite the very long (micrometer) separation between superconducting islands, thus highlighting the presence of triplet superconductivity. We believe this class of 2D weak-link arrays, based of triplet superconductivity, offers much potential for the manipulation of superconductivity based on the spin degree of freedom, which bears both significant fundamental and technological interest.

In this study, we have used a simple approach to fabricate $YBa_2Cu_3O_7/La_{0.7}Ca_{0.3}MnO_3$ planar weak-link arrays. To do so, a single layer of YBCO (24 nm) was grown on top of $SrTiO_3$ (001) by high-oxygen pressure sputtering at 900 °C at $P(O_2) = 3.4$ mbar followed by a 30-min baking at 550 °C at $P(O_2) = 900$ mbar. Subsequently, a 19 × 19 matrix of YBCO micropillars was defined using conventional photolithography and wet etching. The micropillars are $3.5 \times 3.5\ \mu m^2$ in size and are separated by $L = 1.33\ \mu m$. Figure 1(c) displays an AFM image of the YBCO micropillars, which appear well separated excluding the presence of shorts between them. On top of this matrix, a single layer of LCMO (d = 30 nm) was deposited using the same sputtering growth process used for YBCO. Figure 1(a) shows a side-view schematic of the resulting device indicating the dimensions. Figure 1(b) shows a top view of the device, featuring the four-point measurement configuration employed to measure magnetoresistance. In this configuration, current flows across several YBCO micropillars and their respective LCMO spacers, and a magnetic field is applied perpendicular to the current direction.

The resistance vs temperature of the device is depicted in Fig. 1(d). The sharp drop of the resistance at 87.5 K signals the T_c of YBCO. Above it, we observe two maxima of the resistance related to the presence of LCMO. For an LCMO single layer, only one maximum is expected for its characteristic insulator-to-metal transition.[34] The presence of two maxima suggests the existence of two LCMO phases with different metal-to-insulator transitions (MIT), one at $T_{MIT} = 230$ K, close to the one expected for the optimally doped thin layers,[34] and a second one, extremely suppressed, at $T_{MIT} = 130$ K, which might be attributed to variations in the growth process of LCMO (on either STO or YBCO surfaces) or a potential oxygen migration between LCMO and the ab-planes of YBCO.

To further investigate whether these two FM phases are intermixed or spatially separated, we imaged the magnetic domain structure of the S/F array as a function of temperature. We employed photoemission electron microscopy (PEEM), using x-ray magnetic circular dichroism (XMCD) as the magnetic contrast mechanism. The angle of incidence of the incoming x-ray beam is set to 16° with respect to the sample surface with its in-plane projection parallel to the (010) LCMO direction (parallel to one of the edges of the YBCO squares). This configuration ensures large sensitivity to the in-plane magnetization. Images of the array were obtained at the Mn L_3 edge (640.3 eV)

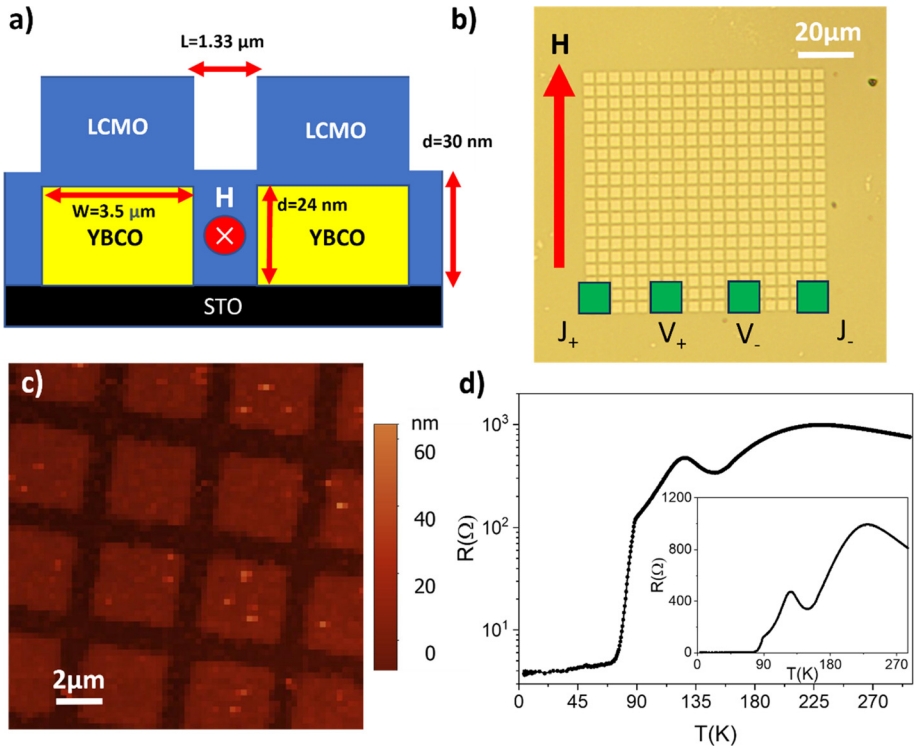

FIG. 1. (a) Sketch of the lateral view of the device structure: YBCO micropillars ($3.5 \times 3.5\ \mu m^2$ and 24 nm thick separated by 1.33 μm) matrix, in yellow, covered by a single layer of LCMO (30 nm), in blue. The central red circle indicates the direction of the field. Current is injected left to right. (b) Measurement configuration and optical microscope image of the device. Green squares indicate where the sputtered gold contacts were deposited to inject current and measure voltage. (c) AFM image of a representative part of the matrix, showing the separation between YBCO micropillars. (d) Resistance vs temperature of the device with a current level of 10 μA. Both the MIT of LCMO and the superconducting transition of YBCO can be observed. Inset: R vs T in linear scale, highlighting the two MITs of LCMO.

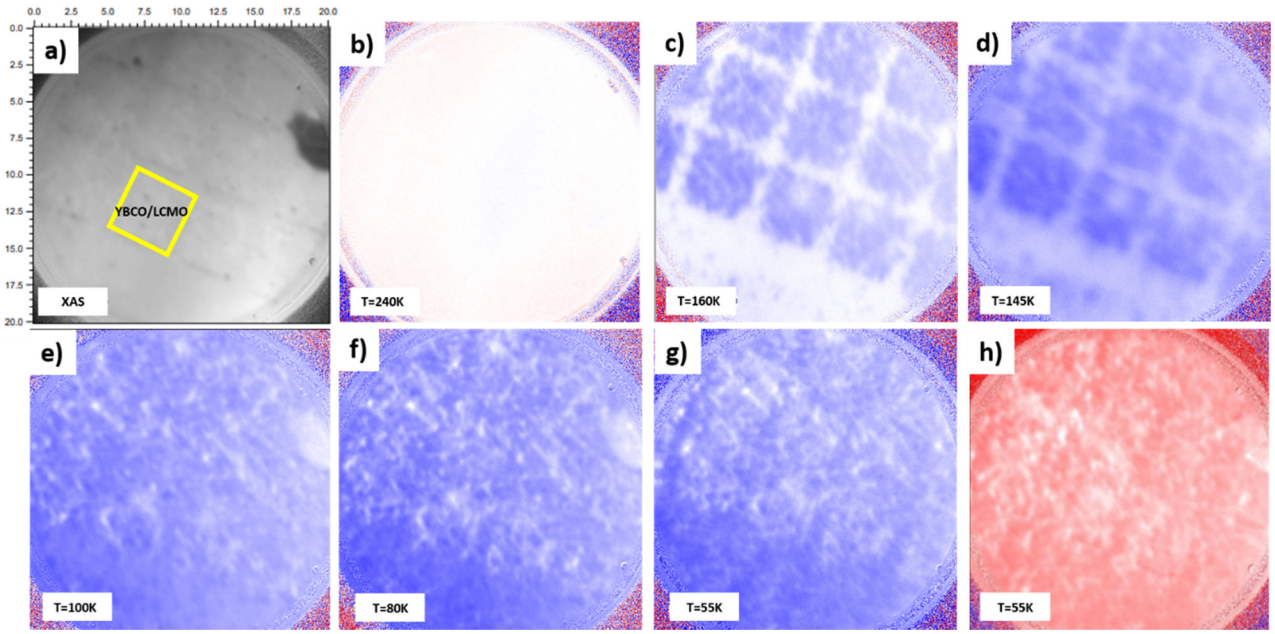

FIG. 2. (a) XAS of the zone to be measured. (b)–(g) XMCD signal evolution in function of temperature after application of 1000 Oe in plane, measured in remanence. Two Curie temperatures can be clearly observed, the one of the LCMO on top of the YBCO and the one of the LCMO between YBCO and outside the YBCO matrix. (h) Reversal of the magnetization after applying −1000Oe in plane, measured in remanence.

with incoming left (σ^-) and right (σ^+) circularly polarized radiation. The XMCD is computed as XMCD $= (\sigma^- - \sigma^+)/(\sigma^- + \sigma^+)$. The blue (red) color scale used to illustrate the resulting XMCD images highlights magnetization parallel (anti-parallel) to the x-ray beam propagation direction. White colored regions, corresponding to XMCD $= 0$, result from regions with zero magnetization or with the magnetization orthogonal to the beam propagation direction. XMCD images were obtained at remanence for different temperatures after applying a 1000 Oe magnetic field pulse (1s) at T = 55K, along the (010) direction. The results are shown in Fig. 2. The temperature-dependent XMCD reveals the existence of two spatially separated ferromagnetic LCMO phases in our system: the LCMO layer on top of YBCO displays a higher Curie temperature, T_{Curie} (between 240 and 160 K) compared to the LCMO located between YBCO micropillars (with T_{Curie} between 145 and 100 K). The XMCD analysis validates the observation from resistance measurements of the presence of two different T_{MIT}, as T_{MIT} and T_{Curie} are linked in manganites.[35,36] It is essential to emphasize that all the LCMO remains ferromagnetic well above and below the critical temperature (87 K) of YBCO.

For a better understanding of the magnetic characteristics of the system, magnetoresistance curves were measured above and below the critical temperature of YBCO. Figure 3(a) displays the magnetoresistance at 90 K, which shows the expected behavior for an LCMO film,[37] anisotropic low-field magnetoresistance (AMR) features (with peaks indicating a coercive field of 20 mT) combined with the negative magnetoresistance background at high field, which corresponds to the colossal magnetoresistance (CMR). Remarkably, as the temperature is decreased below 15 K, the magnetoresistance reveals an oscillating

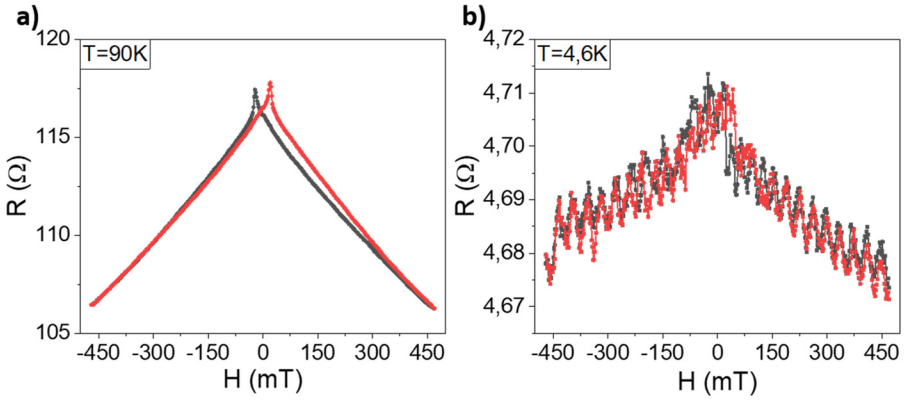

FIG. 3. (a) Magnetoresistance curves with magnetic field applied in plane above Tc of YBCO with I = 60 μA. A typical LCMO magnetoresistance curve is observed, with coercive fields close to 20 mT. (b) Magnetoresistance curves with a magnetic field applied in a plane below the Tc of YBCO. Fraunhofer-like oscillations appear, showing a small hysteretic behavior only at low fields.

pattern, superimposed on the LCMO magnetoresistance, with a periodicity of 37 mT [Fig. 3(b)]. For this composition of the manganite, the low-temperature phase is homogeneous, i.e., it does not show phase separation which is known to be pronounced for other manganites.[38] Here, the only source of inhomogeneity is at the metal to insulator transition, away from the temperature range of the observed resistance oscillations.

Furthermore, the amplitude of the oscillations decreases by increasing either the applied current (above 260 μA) or the temperature (above T = 19 K) of the system, while maintaining the same periodicity [Figs. 4(a) and 4(b)]. This behavior suggests a superconducting origin of these oscillations.

The abrupt resistance drop observed when temperature is reduced below the critical temperature of YBCO [see Fig. 1(d)] is a strong indication of the ferromagnetic/superconducting proximity effect on the LCMO layers. As we discuss on what follows, this resistance drop can only be understood if we assume a strong suppression of the LCMO resistance below that temperature. To probe it, we estimate the expected resistance values at 100 and 4 K in the case of no proximity effect. We start from typical resistivity values for YBCO and LCMO. We will assume that the resistivity of LCMO[34] at 100 K is $\rho_{T=100K} = 0.35$ mΩ cm and at 4 K $\rho_{T=4K} = 0.2$ mΩ cm, and that the resistivity of YBCO is $\rho_{T=100K} = 0.07$ mΩ cm in the normal state and $\rho_{T=4K} = 0$ mΩ cm in the superconducting state, according to the measurements done in single layers. Considering that voltage is measured across three YBCO/LCMO micropillars (with LCMO and YBCO components connected in parallel) connected in a series through the LCMO spacer [see measurement configuration shown in Figs. 1(a) and 1(b) and supplementary material, Fig. S1], we have estimated the resistance at different temperatures with the following formula: $R_{Total} = N \cdot \left(R_{LCMO\,1}/_{YBCO} + R_{LCMO\,2}\right) = N \cdot \left(\frac{R_{LCMO\,1}+R_{YBCO}}{RR_{LCMO\,1}\cdot R_{YBCO}} + R_{LCMO\,2}\right)$, where $R_{LCMO\,1}$ is the resistance of the LCMO on top of YBCO, R_{YBCO} is the resistance of YBCO, and $R_{LCMO\,2}$ is the resistance of the LCMO spacer. N is the total number of devices (i.e., 1 YBCO/LCMO micropillar connected in series with 1 LCMO spacer). Each resistance is calculated by taking into account the resistivity at different temperatures and the dimensions of the devices [as shown in Fig. 1(a)].

At 100 K, the unit cell formed by the bilayer spacer is expected to have an R = 67 Ω. Since our measurement configuration involves N = 3 micropillars [see Fig. 1(b)], the total resistance at 100 K would be $R_{T=100K} = 201$ Ω, a value close to the one experimentally measured $R_{m,T=100K} = 186$ Ω. At 4 K, with the YBCO resistance now reduced to zero, the resistance of the unit cell would be solely due to the LCMO layer. The estimated value is $R_{T=4K} = 76$ Ω, more than one order of magnitude higher than the measured $R_{m,T=4K} \sim 4$ Ω. Even considering a possible conduction in parallel across the 3 × 3 set of micropillars covered by the contacts, the low-temperature resistance state ($R_{T=4K} = 25$ Ω) would still be one order of magnitude above the measured value. This significant difference between the estimated and measured resistances can only be understood if the resistance of the LCMO spacer in between the YBCO/LCMO pillars is significantly reduced by the superconducting proximity effect. In contrast to previous experiments,[23–25] our study did not reveal a zero resistance state, which suggests inhomogeneities across the array.[28] Because the array has multiple YBCO/LCMO/YBCO junctions connected in series, a weaker superconducting proximity effect in one of the junctions along the current path could mask the effects of fully proximized junctions. Another possible explanation for the absence of zero resistance may be related to the degradation of the YBCO micropillars at the edges upon etching [see Fig. 1(c)]. This degradation may result in a decrease in the T_c at the interface in contact with the LCMO, thereby weakening the efficiency of the proximity effect.

One important indication of the superconducting proximity effect is found in the oscillations observed in the magnetoresistance curves. The critical current of a Josephson junction oscillates with the magnetic field according to the well-known Fraunhofer pattern, $I_c(H) = I_{c0}\left|\frac{\sin \pi\frac{\Phi}{\Phi_0}}{\pi\frac{\Phi}{\Phi_0}}\right|$, where $\Phi(H) = \mu_0 H A_{eff}$ is the fmagnetic flux threaded by the junction, I_{c0} is the maximum critical current, and Φ_0 is the flux quantum (2.07×10^{-15} Wb). In fact, the (magnetic field) period of 37 mT of the oscillations observed corresponds to a weak-link area of 0.056 μm^2, which fairly matches the geometry of the LCMO spacers between YBCO pillars. The effective area of the weak link, i.e., the LCMO in between YBCO micropillars [Fig. 1(a)] can be calculated as $A_{eff} = (L + 2\lambda) \cdot d = 0.055\,\mu$m^2, by assuming a value of $\lambda = 250$ nm for the London penetration depth of YBCO when in contact with LCMO.[23] The good agreement between the expected and the measured effective area demonstrates the superconducting nature of the oscillations. As observed, increasing either temperature of the current level decreases the amplitude of the oscillations, making them eventually disappear as expected from the reduction of the critical current. Notice that the magnetoresistance oscillations are not dampened when increasing magnetic field, contrary to conventional single

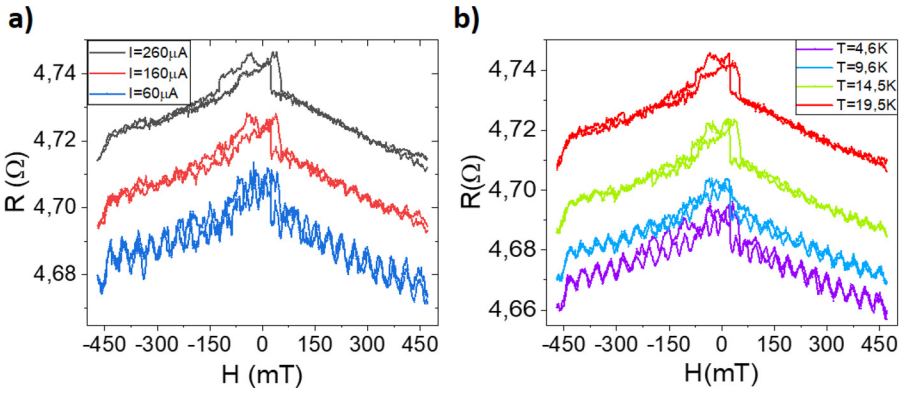

FIG. 4. Magnetoresistance oscillations with a 37 mT period appear below a certain (a) current (at T = 5 K) and (b) temperature threshold (with I = 50 μA). In both cases, the amplitude of the oscillations fades away when either the current (a) or temperature (b) is increased.

Josephson junctions. This type of behavior is expected in Josephson junctions with an inhomogeneous current distribution.[39] For our measurement configuration, the critical current should flow through the upper and lower edges of the LCMO weak link [see Fig. 1(a)]. In fact, a similar effect has been observed in Nb/Co/Nb[40] triplet Josephson junctions, where the long-range triplet correlations appear only in highly localized channels at the edge of the ferromagnet. Fermin *et al.*[40] proposed that this effect is due to the presence of an effective spin–orbit coupling (SOC), originated via non-collinear spin textures present at the barrier.[14,41] This spin–orbit coupling can lead to the appearance of equilibrium triplet Cooper pair spin currents flowing through the edges of the barrier.[14,40–42] This behavior provides further confirmation of the triplet weak-link Josephson junction characteristics in our system, even across a relatively long barrier (1.33 μm) of ferromagnetic LCMO and with smaller widths (3.5 μm) of SC/FM interfaces to generate triplet supercurrents, contrary to our previous works in which their large width could make it difficult to understand how triplet supercurrents are generated.

In summary, we have shown evidence of magnetic flux quantization effects in the resistance of $YBa_2Cu_3O_7/La_{0.7}Ca_{0.3}MnO_3$ weak-link arrays which can be extinguished by either increasing the applied current or temperature. We rationalize these results in terms of a triplet superconducting proximity effect over the micrometer-wide LCMO spacers (1.33 μm) between YBCO micro squares of the array. The matrix of proximized LCMO weak links signals a promising avenue for advanced quantum sensing or logic devices[43] incorporating the spin degree of freedom.[44,45] Overall, the combination of ferromagnets and superconductors in weak-link arrays holds great promise for practical applications in information processing and beyond.

See the supplementary material for a sketch of the resistors' configuration used to calculate the resistance at T = 100K and T = 4K.

Work at UCM was supported by Agencia Estatal de Investigación through Nos. PID2020-118078RB-I00 and TED 2021-130196B-C21, and by Comunidad de Madrid through No. Y2020-NMT6661 (CAIRO). We thank Helmholtz-Zentrum Berlin for the allocation of synchrotron radiation beamtime supported by the project CALIPSOplus under the Grant Agreement No. 730872 from the EU Framework Programme for Research and Innovation HORIZON 2020. Work at Laboratoire Albert Fert supported by ANR-22-EXSP-0007 PEPR SPIN "SPINMAT," by French ANR "SUPERFAST," EU-FLAG-ERA "To2Dox," and COST action "SUPERQUMAP."

AUTHOR DECLARATIONS

Conflict of Interest

The authors have no conflicts to disclose.

Author Contributions

D. Sanchez-Manzano: Conceptualization (lead); Investigation (lead); Methodology (equal); Writing – original draft (lead); Writing – review & editing (equal). **S. Mesoraca:** Investigation (equal); Methodology (equal); Writing – review & editing (equal). **S. Rodriguez-Corvillo:** Investigation (supporting); Methodology (supporting). **A. Lagarrigue:** Investigation (supporting); Methodology (supporting). **F. Gallego:** Investigation (equal); Methodology (supporting). **F. A. Cuellar:** Investigation (supporting); Methodology (supporting). **A. Sander:** Investigation (supporting); Methodology (supporting). **A. Rivera-Calzada:** Investigation (equal); Methodology (equal); Writing – review & editing (equal). **S. Valencia:** Investigation (equal); Methodology (equal); Writing – review & editing (equal). **J. E. Villegas:** Funding acquisition (equal); Supervision (equal); Writing – review & editing (equal). **C. Leon:** Conceptualization (equal); Funding acquisition (equal); Supervision (equal); Writing – review & editing (equal). **J. Santamaria:** Conceptualization (equal); Funding acquisition (lead); Supervision (lead); Writing – review & editing (equal).

DATA AVAILABILITY

The data that support the findings of this study are available from the corresponding author upon reasonable request.

REFERENCES

[1]P. W. Anderson and H. Suhl, "Spin alignment in the superconducting state," Phys. Rev. **116**(4), 898 (1959).
[2]V. S. Stolyarov, I. S. Veshchunov, S. Y. Grebenchuk, D. S. Baranov, I. A. Golovchanskiy, A. G. Shishkin, N. Zhou, Z. Shi, X. Xu, S. Pyon, Y. Sun, W. Jiao, G. H. Cao, L. Y. Vinnikov, A. A. Golubov, T. Tamegai, A. I. Buzdin, and D. Roditchev, "Domain Meissner state and spontaneous vortex-antivortex generation in the ferromagnetic superconductor $EuFe_2(As_{0.79}P_{0.21})_2$," Sci. Adv. **4**(7), eaat1061 (2018).
[3]D. Aoki and J. Flouquet, "Ferromagnetism and superconductivity in uranium compounds," J. Appl. Phys. **81**(1), 011003 (2012).
[4]D. Aoki, A. Huxley, E. Ressouche, D. Braithwaite, J. Flouquet, J.-P. Brison, E. Lhotel, and C. Paulsen, "Coexistence of superconductivity and ferromagnetism in URhGe," Nature **413**(6856), 613–616 (2001).
[5]L. Jiao, S. Howard, S. Ran, Z. Wang, J. O. Rodriguez, M. Sigrist, Z. Wang, N. P. Butch, and V. Madhavan, "Chiral superconductivity in heavy-fermion metal UTe_2," Nature **579**(7800), 523–527 (2020).
[6]S. Ran, C. Eckberg, Q. P. Ding, Y. Furukawa, T. Metz, S. R. Saha, I. L. Liu, M. Zic, H. Kim, J. Paglione, and N. P. Butch, "Nearly ferromagnetic spin-triplet superconductivity," Science **365**(6454), 684–687 (2019).
[7]M. Eschrig and T. Löfwander, "Triplet supercurrents in clean and disordered half-metallic ferromagnets," Nat. Phys. **4**(2), 138–143 (2008).
[8]M. Eschrig, "Spin-polarized supercurrents for spintronics: A review of current progress," Rep. Prog. Phys. **78**(10), 104501 (2015).
[9]M. Eschrig, J. Kopu, J. C. Cuevas, and G. Schön, "Theory of half-metal/superconductor heterostructures," Phys. Rev. Lett. **90**(13), 137003 (2003).
[10]M. Houzet and A. I. Buzdin, "Long range triplet Josephson effect through a ferromagnetic trilayer," Phys. Rev. B **76**(6), 060504 (2007).
[11]C. Richard, M. Houzet, and J. S. Meyer, "Superharmonic long-range triplet current in a diffusive Josephson junction," Phys. Rev. Lett. **110**(21), 217004 (2013).
[12]F. S. Bergeret, A. F. Volkov, and K. B. Efetov, "Long-range proximity effects in superconductor-ferromagnet structures," Phys. Rev. Lett. **86**(18), 4096–4099 (2001).
[13]F. S. Bergeret, A. F. Volkov, and K. B. Efetov, "Odd triplet superconductivity and related phenomena in superconductor-ferromagnet structures," Rev. Mod. Phys. **77**(4), 1321–1373 (2005).
[14]F. S. Bergeret and I. V. Tokatly, "Singlet-triplet conversion and the long-range proximity effect in superconductor-ferromagnet structures with generic spin dependent fields," Phys. Rev. Lett. **110**(11), 117003 (2013).
[15]J. W. A. Robinson, J. D. S. Witt, and M. G. Blamire, "controlled injection of spin-triplet supercurrents into a strong ferromagnet," Science **329**(5987), 59–61 (2010).
[16]T. S. Khaire, M. A. Khasawneh, W. P. Pratt, and N. O. Birge, "Observation of spin-triplet superconductivity in co-based Josephson junctions," Phys. Rev. Lett. **104**(13), 137002 (2010).
[17]E. C. Gingrich, B. M. Niedzielski, J. A. Glick, Y. Wang, D. L. Miller, R. Loloee, W. P. Pratt, and N. O. Birge, "Controllable 0-π Josephson junctions containing a ferromagnetic spin valve," Nat. Phys. **12**(6), 564–567 (2016).

[18]C. Visani, Z. Sefrioui, J. Tornos, C. Leon, J. Briatico, M. Bibes, A. Barthélémy, J. Santamaría, and J. E. Villegas, "Equal-spin Andreev reflection and long-range coherent transport in high-temperature superconductor/half-metallic ferromagnet junctions," Nat. Phys. **8**(7), 539–543 (2012).
[19]Y. Kalcheim, T. Kirzhner, G. Koren, and O. Millo, "Long-range proximity effect in $La_{2/3}Ca_{1/3}MnO_3$/(100)$YBa_2Cu_3O_{7-\delta}$ ferromagnet/superconductor bilayers: Evidence for induced triplet superconductivity in the ferromagnet," Phys. Rev. B **83**(6), 064510 (2011).
[20]K. Dybko, K. Werner-Malento, P. Aleshkevych, M. Wojcik, M. Sawicki, and P. Przyslupski, "Possible spin-triplet superconducting phase in the $La_{0.7}Sr_{0.3}MnO_3$/$YBa_2Cu_3O_7$/$La_{0.7}Sr_{0.3}MnO_3$ trilayer," Phys. Rev. B **80**(14), 144504 (2009).
[21]R. S. Keizer, S. T. B. Goennenwein, T. M. Klapwijk, G. Miao, G. Xiao, and A. Gupta, "A spin triplet supercurrent through the half-metallic ferromagnet CrO_2," Nature **439**(7078), 825–827 (2006).
[22]M. S. Anwar, F. Czeschka, M. Hesselberth, M. Porcu, and J. Aarts, "Long-range supercurrents through half-metallic ferromagnetic CrO_2," Phys. Rev. B **82**(10), 100501 (2010).
[23]D. Sanchez-Manzano, S. Mesoraca, F. A. Cuellar, M. Cabero, V. Rouco, G. Orfila, X. Palermo, A. Balan, L. Marcano, A. Sander, M. Rocci, J. Garcia-Barriocanal, F. Gallego, J. Tornos, A. Rivera, F. Mompean, M. Garcia-Hernandez, J. M. Gonzalez-Calbet, C. Leon, S. Valencia, C. Feuillet-Palma, N. Bergeal, A. I. Buzdin, J. Lesueur, J. E. Villegas, and J. Santamaria, "Extremely long-range, high-temperature Josephson coupling across a half-metallic ferromagnet," Nat. Mater. **21**(2), 188–194 (2022).
[24]D. Sanchez-Manzano, S. Mesoraca, F. A. Cuellar, M. Cabero, S. Rodriguez-Corvillo, V. Rouco, F. Mompean, M. Garcia-Hernandez, J. M. Gonzalez-Calbet, C. Feuillet-Palma, N. Bergeal, J. Lesueur, C. Leon, J. E. Villegas, and J. Santamaria, "Unconventional long range triplet proximity effect in planar $YBa_2Cu_3O_7$/$La_{0.7}Sr_{0.3}MnO_3$/$YBa_2Cu_3O_7$ Josephson junctions," Supercond. Sci. Technol. **36**(7), 074002 (2023).
[25]Y. Jungxiang, R. Fermin, K. Lahabi, and J. Aarts, "Triplet supercurrents in lateral Josephson junctions with a half-metallic ferromagnet," arXiv:2303.13922v1 (2023).
[26]T. Yamashita, K. Tanikawa, S. Takahashi, and S. Maekawa, "Superconducting π qubit with a ferromagnetic Josephson junction," Phys. Rev. Lett. **95**(9), 097001 (2005).
[27]J. Linder and J. W. A. Robinson, "Superconducting spintronics," Nat. Phys. **11**(4), 307–315 (2015).
[28]S. Eley, S. Gopalakrishnan, P. M. Goldbart, and N. Mason, "Approaching zero-temperature metallic states in mesoscopic superconductor–normal–superconductor arrays," Nat. Phys. **8**(1), 59–62 (2012).
[29]Z. Han, A. Allain, H. Arjmandi-Tash, K. Tikhonov, M. Feigel'Man, B. Sacépé, and V. Bouchiat, "Collapse of superconductivity in a hybrid tin–graphene Josephson junction array," Nat. Phys. **10**(5), 380–386 (2014).
[30]C. G. L. Bøttcher, F. Nichele, M. Kjaergaard, H. J. Suominen, J. Shabani, C. J. Palmstrøm, and C. M. Marcus, "Superconducting, insulating and anomalous metallic regimes in a gated two-dimensional semiconductor–superconductor array," Nat. Phys. **14**(11), 1138–1144 (2018).
[31]S. Mukhopadhyay, J. Senior, J. Saez-Mollejo, D. Puglia, M. Zemlicka, J. M. Fink, and A. P. Higginbotham, "Superconductivity from a melted insulator in Josephson junction arrays," Nat. Phys. **19**, 1630–1636 (2023).
[32]D. J. Resnick, J. C. Garland, J. T. Boyd, S. Shoemaker, and R. S. Newrock, "Kosterlitz-Thouless transition in proximity-coupled superconducting arrays," Phys. Rev. Lett. **47**(21), 1542–1545 (1981).
[33]D. W. Abraham, C. J. Lobb, M. Tinkham, and T. M. Klapwijk, "Resistive transition in two-dimensional arrays of superconducting weak links," Phys. Rev. B **26**(9), 5268–5271 (1982).
[34]N. M. Nemes, M. García-Hernández, Z. Szatmári, T. Fehér, F. Simon, C. Visani, V. Peña, C. Miller, J. García-Barriocanal, F. Bruno, Z. Sefrioui, C. Leon, and J. Santamaría, "Thickness dependent magnetic anisotropy of ultrathin LCMO epitaxial thin films," IEEE Trans. Magn. **44**(11), 2926–2929 (2008).
[35]A. Urushibara, Y. Moritomo, T. Arima, A. Asamitsu, G. Kido, and Y. Tokura, "Insulator-metal transition and giant magnetoresistance in $La_{1-x}Sr_xMnO_3$," Phys. Rev. B **51**(20), 14103 (1995).
[36]M. B. Salamon and M. Jaime, "The physics of manganites: Structure and transport," Rev. Mod. Phys. **73**(3), 583 (2001).
[37]M. Ziese, H. C. Semmelhack, K. H. Han, S. P. Sena, H. J. Blythe, K. H. Semmelhack, S. P. Han, H. J. Sena, and H. C. Blythe, "Thickness dependent magnetic and magnetotransport properties of strain-relaxed $La_{0.7}Ca_{0.3}MnO_3$ films," J. Appl. Phys. **91**(12), 9930–9936 (2002).
[38]K. A. Moler, "Imaging quantum materials," Nat. Mater. **16**(11), 1049–1052 (2017).
[39]A. Barone and G. Paternò, *Physics and Applications of the Josephson Effect* (Wiley, 1982).
[40]R. Fermin, D. Van Dinter, M. Hubert, B. Woltjes, M. Silaev, J. Aarts, and K. Lahabi, "Superconducting triplet rim currents in a spin-textured ferromagnetic disk," Nano Lett. **22**(6), 2209–2216 (2022).
[41]I. V. Bobkova and Y. S. Barash, "Effects of spin-orbit interaction on superconductor-ferromagnet heterostructures: Spontaneous electric and spin surface currents," JETP Lett. **80**(7), 494–499 (2004).
[42]F. S. Bergeret and I. V. Tokatly, "Spin-orbit coupling as a source of long-range triplet proximity effect in superconductor-ferromagnet hybrid structures," Phys. Rev. B **89**(13), 134517 (2014).
[43]L. B. Ioffe, M. V. Feigel'man, A. Ioselevich, D. Ivanov, M. Troyer, and G. Blatter, "Topologically protected quantum bits using Josephson junction arrays," Nature **415**(6871), 503–506 (2002).
[44]J. Oppenländer, C. Häussler, and N. Schopohl, "Non−Φ_0−periodic macroscopic quantum interference in one-dimensional parallel Josephson junction arrays with unconventional grating structure," Phys. Rev. B **63**(2), 024511 (2000).
[45]F. Couëdo, E. Recoba Pawlowski, J. Kermorvant, J. Trastoy, D. Crété, Y. Lemaître, B. Marcilhac, C. Ulysse, C. Feuillet-Palma, N. Bergeal, and J. Lesueur, "High-TC superconducting detector for highly-sensitive microwave magnetometry," Appl. Phys. Lett. **114**(19), 192602 (2019).